Preprints of the 21st IFAC World Congress (Virtual)
Berlin, Germany, July 12-17, 2020

Nonlinear control formulation based on sliding mode control applied to a 2-DOF control moment gyroscope

Gobiha D*, Rohith G, Nandan K Sinha*****

*Research Scholar, Department of Aerospace Engineering (e-mail: gobiha@yahoo.com)
**Research Scholar, Department of Aerospace Engineering (e-mail: rohith044@gmail.com)
***Professor, Department of Aerospace Engineering (e-mail: nandan@ae.iitm.ac.in)

Indian Institute of Technology Madras, Chennai – 600036, India

Abstract: Though conceptualization of nonlinear sliding mode control has gained great emphasis in mechatronics and nonlinear systems in general, little attention is given to real time implementation owing to its inadequacy in handling mismatched uncertainties. This work contemplates on a robust nonlinear control scheme with sliding mode control and extended Kalman filter in closed-loop to estimate and handle bounded uncertainties. Stability of this closed-loop framework is established through Lyapunov analysis. The proposed formulation is first validated on a simulation platform and then implemented on a 2-DOF experimental gyroscope setup. Efficacy of this approach is evident from its rigorous tracking performance attained with a smooth and bounded control profile, despite induced uncertainties in various forms.

Keywords: Gyroscope, nonlinear sliding mode control, uncertainties, real time experiments.

1. INTRODUCTION

Recent years have seen a significant upsurge of interest among control research fraternity on nonlinear control system design and development. This is primarily attributed to the increasing power of computing resources combined with an urge to understand the dynamical behaviour of real time systems completely, which is otherwise not captured in linearized models (Sastry, 1999). Although nonlinear controllers are excessively abstracted, implementation on real time systems are rarely dealt with, thereby questioning the feasibility of nonlinear controllers when applied to real time systems. This work therefore focuses on analyzing the performance of a real time experimental gyroscope setup to a nonlinear control framework designed using sliding mode control (SMC).

Gyroscopes have great importance in aerial vehicle guidance, navigation and control. These devices act as an attitude sensor when mounted on a rotating frame by sensing its angular velocity. Thus, they are an integral part of gyrocompasses, inertial measurement and navigation units. Control moment gyroscopes (CMGs) owing to its rapid rotational maneuverability could also be used as primary actuating devices in aerial vehicles, space vehicles, satellites and international space station to maintain their attitude in space.

Most works on nonlinear control strategies discussed in literature predominantly uses either nonlinear sliding mode control or nonlinear model predictive control, with few focusing on nonlinear dynamic inversion techniques, backstepping and other Lyapunov based control formulations. Literature pertaining to nonlinear control of CMGs is briefed in this section. Attitude control of spacecraft installed with a single gimbal CMG using nonlinear backstepping control is formulated in Jin and Hwang (2012) and Elkhayat et al. (2016). Extension of this framework using nonlinear robust backstepping algorithm for agile satellites fitted with a double gimbal, variable speed CMG is evaluated in Zhang and Fang (2013). Lyapunov based nonlinear control formulation for limited three dimensional attitude control is proposed in Stevenson and Schaub (2012) for a spacecraft mounted with a double gimbal, variable speed CMG. An adaptive neural quaternion based feedback control law is adapted for attitude control of spacecraft (Leeghim and Kim, 2015). Naderolasli and Tabatabaei (2017) consider stabilization of a two degrees of freedom (DOF) gyroscope platform based on adaptive fractional order sliding mode controller. Attitude stabilization of satellites based on dynamic sliding mode control for faster convergence rate with consideration on angular velocity and control constraints is proposed in Yu and Xie (2019). Even though all these nonlinear control techniques are assessed using numerical simulations, real time implementation has not been considered.

With the availability of the experimental 3-DOF gyroscope setup by Quanser, real time implementation and validation of the proposed control techniques become quite convenient. An adaptive model based algorithm for the control of 2-DOF CMG is proposed in Montoya-Cháirez et al. (2019). Though nonlinear adaptive control scheme has been proposed, performance evaluation in real time with the experimental Quanser setup in closed-loop uses only linear control law (Montoya-Cháirez et al., 2019). A relay periodic switching function based control of 2-DOF CMG is carried out in Oliveira et al. (2015). Besides using a linear model, this method also suffers from chattering due to relay periodic switching function (Oliveira et al., 2015).

Though nonlinear controls are theoretically more convincing and elegant than its linear counterparts, they are vaguely beneficial if they cannot be implemented on uncertain real time systems. Real time systems suffer from model mismatch along

with process and measurement noise; thus, robustness of the controller should be of utmost concern. Though sliding mode based controllers are known for its robustness in handling matched uncertainties (Slotine and Li, 1991), it is ineffective in handling mismatched uncertainties i.e. when uncertainties act through different channels from that of input channel (Hou et al., 2017; Yang et al., 2013). Adaptive and LMI based approaches are widely employed to handle mismatched uncertainties. But these techniques do not handle uncertainties with nonzero steady state values. Integral SMC provides a simpler approach to mismatched uncertainties, but integral action might affect the control performance. In Yang et al., (2013), disturbance estimate from disturbance observer is used in sliding surface to handle mismatched uncertainties and simulation results show nominal performance recovery. In that context, extended Kalman filter (EKF) which has proven to be an effective real time estimator for industrial applications is used. Utilization of dynamic model in EKF formulation improves the overall robustness of the control system. Thus, this work integrates nonlinear SMC and EKF framework to estimate and handle system uncertainties effectively. This approach retains the nominal performance of SMC while accounting for uncertainties. Stability of the proposed closed-loop framework is established using Lyapunov analysis. Real time performance is evaluated by implementing on a gyroscope test bed. Besides process and measurement noise, mass addition to vary gimbal's moment of inertia and vibratory disturbance are induced to assess its performance in detrimental conditions.

This paper is organized as follows. Section 2 briefs the dynamic modeling of the considered experimental 2-DOF gyroscope platform. Proposed closed-loop architecture with emphasis on nonlinear SMC formulation and stability analysis is described in Section 3. Section 4 discusses the simulated and experimental results while Section 5 concludes the paper.

2. DYNAMIC MODEL OF 2-DOF GYROSCOPE

A 3-DOF gyroscope of Quanser pictured in Fig. 1 has been used as an experimental test bed. This system consists of a rotating disc mounted in an inner blue gimbal, supported by an outer red gimbal and a rectangular frame. Each of these gimbals and the frame are free to rotate about their rotational axes while the speed of the rotating disc is maintained constant. This makes it a 3-DOF system. Based on the applicability of the system, either the gimbals or the frame is fixed in place, thereby reducing its degree of freedom. In this work, rectangular frame is fixed resulting in a 2-DOF system.

Fig. 1 Gyroscope test bed

The dynamic equations of 2-DOF gyroscope (Cannon Jr., 2003) with torque, τ_2 applied along blue gimbal are given by,

$$\begin{aligned} &J_3\ddot{\theta} + h\dot{\psi}\cos\theta - J_a\dot{\psi}^2\sin\theta\cos\theta = \tau_2 \\ &(J_2 + J_a\sin^2\theta)\ddot{\psi} - h\dot{\theta}\cos\theta + J_a\dot{\psi}\dot{\theta}\sin 2\theta = 0 \end{aligned} \tag{1}$$

where θ is the angular position of the blue gimbal with respect to the red gimbal, ψ is the angular position of the red gimbal with respect to the surface on which the gyroscope is mounted. $\dot{\theta}$ and $\dot{\psi}$ are their corresponding angular rates. Angular positions of the gimbal are measured by optical encoders. As velocity sensor is not equipped, angular rates are obtained by processing it with a filter. h is the angular momentum of rotor with respect to blue gimbal. J_x, J_2 and J_3 are the moment of inertia of the rotor, outer and inner gimbal about their respective spin axis, J_a is defined as $J_1 - J_x$, with J_1 being the moment of inertia of outer gimbal excluding the moment of inertia contribution from rectangular frame. The equations of motion for the 2-DOF gyroscope with state vector, $\boldsymbol{x} = [\theta, \dot{\theta}, \psi, \dot{\psi}]'$ and control variable, $u = \tau_2$ are given in Eq. (2).

$$\begin{aligned} \dot{x}_1 &= \dot{\theta} \\ \dot{x}_2 &= \frac{1}{J_3}\left[u + J_a\dot{\psi}^2\sin\theta\cos\theta - h\dot{\psi}\cos\theta\right] \\ \dot{x}_3 &= \dot{\psi} \\ \dot{x}_4 &= \frac{1}{J_2 + J_a\sin^2\theta}\left[h\dot{\theta}\cos\theta - 2J_a\dot{\psi}\dot{\theta}\sin\theta\cos\theta\right] \end{aligned} \tag{2}$$

Moment of inertia values of the considered gyroscope are detailed in Montoya-Cháirez et al. (2019). It is evident that the equations of motion represented by four first order nonlinear differential equations in Eq. (2) are in control affine form.

$$\dot{\boldsymbol{x}} = \boldsymbol{f}(\boldsymbol{x}) + \Delta\boldsymbol{f}(\boldsymbol{x}) + \boldsymbol{g}u; \quad y = h(\boldsymbol{x}) = \psi \tag{3}$$

where $\boldsymbol{f}(\boldsymbol{x})$ is a vector of nonlinear functions characterizing the system and $\boldsymbol{g}$ is the input vector represented in Eq. (4). $\Delta\boldsymbol{f}(\boldsymbol{x})$ represents bounded uncertainties.

$$\boldsymbol{g} = \begin{bmatrix} 0 \\ \frac{1}{J_3} \\ 0 \\ 0 \end{bmatrix}$$

$$\boldsymbol{f}(\boldsymbol{x}) = \begin{bmatrix} x_2 \\ \frac{1}{J_3}\left[J_a {x_4}^2 \sin x_1 \cos x_1 - h x_4 \cos x_1\right] \\ x_4 \\ \frac{1}{J_2 + J_a \sin^2 x_1}\left[h x_2 \cos x_1 - J_a x_4 x_2 \sin 2x_1\right] \end{bmatrix} \tag{4}$$

3. NONLINEAR CONTROLLER DESIGN

Sliding mode control has gained predominant interest among nonlinear research fraternity primarily because of its robustness in handling modeled and unmodeled uncertainties. Sliding mode control is basically a variable structure control with switching logic encompassed in sliding surface. Thus, sliding surface should be promptly chosen such that the trajectories from any arbitrary state tend towards the sliding

surface and remain in it henceforth. This condenses solving a higher order nonlinear system to algebraic equations of reduced order. But, because of discontinuity in variable structure, chattering phenomena could hinder the applicability of SMC. Thus, chattering alleviation is mandatory for successful implementation of sliding mode controller in real time experimental setup. In this work, chattering is alleviated using power rate reaching law (Gao and Hung, 1993).

The primary objective of this work is to generate a control signal, $u(t)$ such that angular position of the red gimbal, $\psi(t)$ converges to the specified reference trajectory, $\psi_d(t)$ while all other states remain bounded, ensuring system stability.

3.1 Sliding mode control formulation

From Lie derivative perspective, γ is the relative degree of the system if,

$$\begin{aligned} L_{\boldsymbol{g}} L_{\boldsymbol{f}}^{i-1} h(\boldsymbol{x}) = 0, \text{ for } i = 1, 2, \dots (\gamma - 1) \\ L_{\boldsymbol{g}} L_{\boldsymbol{f}}^{\gamma-1} h(\boldsymbol{x}) \neq 0 \end{aligned} \tag{5}$$

where the Lie derivative, $L_{\boldsymbol{f}} h$ and $L_{\boldsymbol{g}} h$ are the scalar functions defined as the derivative of h with respect to $\boldsymbol{f}$ and $\boldsymbol{g}$ respectively. In other words, ψ should be differentiated thrice to arrive at an explicit relationship between control, u and output, ψ. Thus, the relative degree of the system is three for the considered 2-DOF gyroscope. As relative degree is less than the order of the system, Eq. (3) could be transformed into a normal form (Khatri et al., 2012; Singh, 1989) using the state vector, $\boldsymbol{z}$ defined as,

$$\boldsymbol{z} = \left[\psi, \dot{\psi}, \ddot{\psi}\right]' \tag{6}$$

Thus, transformed equations of motion in normal form with mismatched and matched uncertainties are given by,

$$\begin{aligned} \dot{z}_1 &= L_{\boldsymbol{f}} h(\boldsymbol{x}) + L_{\Delta \boldsymbol{f}} h(\boldsymbol{x}) \\ \dot{z}_2 &= L_{\boldsymbol{f}}^2 h(\boldsymbol{x}) + L_{\Delta \boldsymbol{f}} L_{\boldsymbol{f}} h(\boldsymbol{x}) \\ \dot{z}_3 &= L_{\boldsymbol{f}}^3 h(\boldsymbol{x}) + L_{\Delta \boldsymbol{f}} L_{\boldsymbol{f}}^2 h(\boldsymbol{x}) + L_{\boldsymbol{g}} L_{\boldsymbol{f}}^2 h(\boldsymbol{x}) u \end{aligned} \tag{7}$$

Concisely, Eq. (7) could be conveniently expressed as,

$$\dot{\boldsymbol{z}} = M\boldsymbol{z} + N(\tilde{f} + \tilde{g}u) + \Delta\tilde{\boldsymbol{f}} \tag{8}$$

with transformed vectors $\tilde{f}$, $\Delta\tilde{\boldsymbol{f}}$ and $\tilde{g}$ defined as,

$$\tilde{f} = L_{\boldsymbol{f}}^3 h(\boldsymbol{x});\ \tilde{g} = L_{\boldsymbol{g}} L_{\boldsymbol{f}}^2 h(\boldsymbol{x});\ \Delta\tilde{\boldsymbol{f}} = \begin{bmatrix} L_{\Delta \boldsymbol{f}} h(\boldsymbol{x}) \\ L_{\Delta \boldsymbol{f}} L_{\boldsymbol{f}} h(\boldsymbol{x}) \\ L_{\Delta \boldsymbol{f}} L_{\boldsymbol{f}}^2 h(\boldsymbol{x}) \end{bmatrix} \tag{9}$$

M and N could be easily shown to be the matrices of dimensions $(\gamma * \gamma)$ and $(\gamma * 1)$,

$$M = \begin{bmatrix} 0 & 1 & 0 \\ 0 & 0 & 1 \\ 0 & 0 & 0 \end{bmatrix};\ N = \begin{bmatrix} 0 \\ 0 \\ 1 \end{bmatrix} \tag{10}$$

Let the desired reference trajectory be represented as,

$$\boldsymbol{r} = \left[\psi_d, \dot{\psi}_d, \ddot{\psi}_d\right]' \tag{11}$$

Thus, the error vector could be specified as,

$$\boldsymbol{e} = \begin{bmatrix} e \\ \dot{e} \\ \ddot{e} \end{bmatrix} = \begin{bmatrix} \psi - \psi_d \\ \dot{\psi} - \dot{\psi}_d \\ \ddot{\psi} - \ddot{\psi}_d \end{bmatrix} \tag{12}$$

The chosen sliding surface, s is shown in Eq. (13). It should be noted that the sliding surface converges to zero as error approaches zero.

$$s = k_1 e + k_2 \dot{e} + \ddot{e} \tag{13}$$

In Eq. (13), k_1, k_2 and k_3 are positive constants. On differentiating Eq. (14) with respect to time,

$$\dot{s} = k_1 \dot{e} + k_2 \ddot{e} + \dddot{e} \tag{14}$$

which could be condensed as,

$$\dot{s} = S_1 \boldsymbol{e} + S_2 \dot{\boldsymbol{e}} \tag{15}$$

with S_1 and S_2 given by,

$$\begin{aligned} S_1 &= [0 \quad k_1 \quad k_2] \\ S_2 &= [0 \quad 0 \quad 1] \end{aligned} \tag{16}$$

On substituting Eq. (8) in Eq. (15),

$$\dot{s} = S_1 \boldsymbol{e} + S_2\left[M\boldsymbol{z} + N\left(\tilde{f} + \tilde{g}u\right) + \Delta\tilde{\boldsymbol{f}} - \dot{\boldsymbol{r}}\right] \tag{17}$$

It could be easily seen that, $S_2 M = 0$ and $S_2 N = 1$. Thus, Eq. (17) becomes,

$$\dot{s} = S_1 \boldsymbol{e} + \tilde{f} + \tilde{g}u + S_2 \Delta\tilde{\boldsymbol{f}} - S_2 \dot{\boldsymbol{r}} \tag{18}$$

As $\dot{s}$ should be a decreasing function and uncertainty is unknown, control input, u derived from Eq. (18) is,

$$u = (\tilde{g})^{-1}\left[-\tilde{f} + S_2 \dot{\boldsymbol{r}} - S_1 \boldsymbol{e} - k(s) sign(s)\right] \tag{19}$$

From Eq. (9), on evaluating $\tilde{g}$, it could be inferred that it is invertible except at $\theta = \pm\pi/2$. This refrains from singularity of control signal as θ is comparatively small in $\psi \in [-\pi, \pi)$. As evident from Eq. (19), continuous change of sign in control signal leads to undesired chattering phenomena. Effect of chattering is mitigated by designing $k(s)$ using power rate reaching law (Gao and Hung, 1993), thereby improving the performance of controller, while ensuring the safety of system actuator. Power rate reaching law is described below,

$$k(s) = \epsilon |s|^{\beta} \text{ where } \epsilon > 0 \text{ and } \beta \in (0,1) \tag{20}$$

Thus, Eq. (19) becomes,

$$u = (\tilde{g})^{-1}\left[-\tilde{f} + S_2 \dot{\boldsymbol{r}} - S_1 \boldsymbol{e} - \epsilon |s|^{\beta}\, sign(s)\right] \tag{21}$$

3.2 Closed-loop architecture

Formulation of controller in closed-loop is visualized as a block diagram in Fig. 2. Simulation platform is embedded in parallel with real time experimentation framework for the ease of comparison. Reference trajectory, $\boldsymbol{r} = [\psi_d, \dot{\psi}_d, \ddot{\psi}_d]'$ is fed to controller blocks. Controller blocks use nonlinear SMC formulation to compute the control signal required to achieve the desired reference trajectory, represented by u_s and u for simulated and real time experimental setup respectively.

Control signals are passed through actuator dynamics block where signals are limited to its saturation value of ± 1.5 Nm to ensure system safety. Trimmed control signals, $\hat{u}_s$ and u are fed to nonlinear gyroscope model presented in Eq. (2) and experimental gyroscope setup respectively. In case of simulation scenario, states from simulated gyroscope model are fed back to the controller. However, states from real time gyroscope platform are affected by factors like measurement and process noise and other uncertainties. Sometimes, a sudden high frequency noise may disorient the entire control framework, thereby collapsing the system. Besides, as evident from Eqs. (18) and (19), SMC could handle only matched uncertainties by proper tuning of $k(s)$. Thus, estimation of states becomes mandatory and the estimated states, $\hat{\boldsymbol{x}}$ is fed back to the controller. In this work, EKF is utilized and its mathematical framework is presented in a nutshell.

Extended Kalman filtering is a recursive approach with two phases, namely prediction and correction. EKF algorithm (Lee and Ricker, 1994) for a system of form specified in Eq. (3) is illustrated in Eqs. (22) and (23), representing prediction and correction stages respectively. Prediction step also called as data fusion, predicts the current state of the system $(\hat{\boldsymbol{x}}_{k|k-1})$ by using its computed mathematical model and state estimates from the previous instance $(\hat{\boldsymbol{x}}_{k-1|k-1})$, while also estimating the error covariance matrix, $(P_{k|k-1})$.

$$\begin{aligned} \hat{\boldsymbol{x}}_{k|k-1} &= \boldsymbol{f}\left(\hat{\boldsymbol{x}}_{k-1|k-1}\right) + \boldsymbol{g}u_k \\ P_{k|k-1} &= F_k P_{k-1|k-1} F_k{}' + Q \end{aligned} \tag{22}$$

In the above equations, Q is the process noise covariance and $F_k = \left.\frac{\partial \boldsymbol{f}}{\partial \boldsymbol{x}}\right|_{(\hat{\boldsymbol{x}}_{k-1|k-1}, u_k)}$ is the state transition matrix.

$$\begin{aligned} K_k &= P_{k|k-1} C' (C P_{k|k-1} C' + R)^{-1} \\ \hat{\boldsymbol{x}}_{k|k} &= \hat{\boldsymbol{x}}_{k|k-1} + K_k\left(\boldsymbol{y}_k - C\hat{\boldsymbol{x}}_{k|k-1}\right) \\ P_{k|k} &= (I - K_k C) P_{k|k-1} \end{aligned} \tag{23}$$

Correction step or sensor fusion, refines the predicted states based on sensor measurements $(\boldsymbol{y}_k)$, by computing Kalman gain (K_k) based on estimated error covariance and measurement noise covariance (R). This step further updates the error covariance matrix $(P_{k|k})$. As first order filter is used to obtain angular rates from the measured angular position, measurement matrix (C) is taken as an identity matrix. Besides providing estimated states in the presence of system disturbances, EKF also provides a better estimates of angular rates which are not directly measurable.

3.3 Closed-loop Lyapunov stability analysis

By imparting the estimated states computed from EKF algorithm onto SMC formulation, Eq. (21) could be written as,

$$u = (\tilde{g})^{-1}\left[-\tilde{f}(\hat{\boldsymbol{x}}) + S_2\dot{\boldsymbol{r}} - S_1\boldsymbol{e} - \epsilon|s|^{\beta}\, sign(s)\right] \tag{24}$$

It should be noted that error computation is based on measured states rather than estimated states to ensure offset free tracking. To assure stability of the proposed controller, chosen sliding surface in Eq. (13) should guarantee attractiveness and finite time reachability. This is established using the following Lyapunov function candidate,

$$V = \frac{1}{2}s^2 > 0, \qquad \forall s \neq 0 \tag{25}$$

Differentiating Eq. (25) with respect to time and on substituting Eq. (18), $\dot{V}$ becomes,

$$\dot{V} = s\left[S_1\boldsymbol{e} + \tilde{f} + \tilde{g}u + S_2\Delta\tilde{\boldsymbol{f}} - S_2\dot{\boldsymbol{r}}\right] \tag{26}$$

Incorporating the derived control signal in Eq. (22) and simplifying Eq. (26),

$$\dot{V} = s\left[\tilde{f} + S_2\Delta\tilde{\boldsymbol{f}} - \tilde{f}(\hat{\boldsymbol{x}}) - \epsilon|s|^{\beta}\, sign(s)\right] \tag{27}$$

As estimated states helps in capturing the dynamics of system in the presence of uncertainties, a recursively computed Kalman gain as in Eq. (23) could effectively handle bounded $\Delta\tilde{\boldsymbol{f}}$, provided convergence of EKF is ensured. Thus, an appropriate Kalman gain guarantees,

$$\dot{V} < -\epsilon|s|^{\beta+1} \tag{28}$$

Equation (28) clearly infers that $\dot{V} < 0$, for $\forall s \neq 0$. This assures asymptotic stability of the proposed closed-loop control framework with the chosen sliding surface.

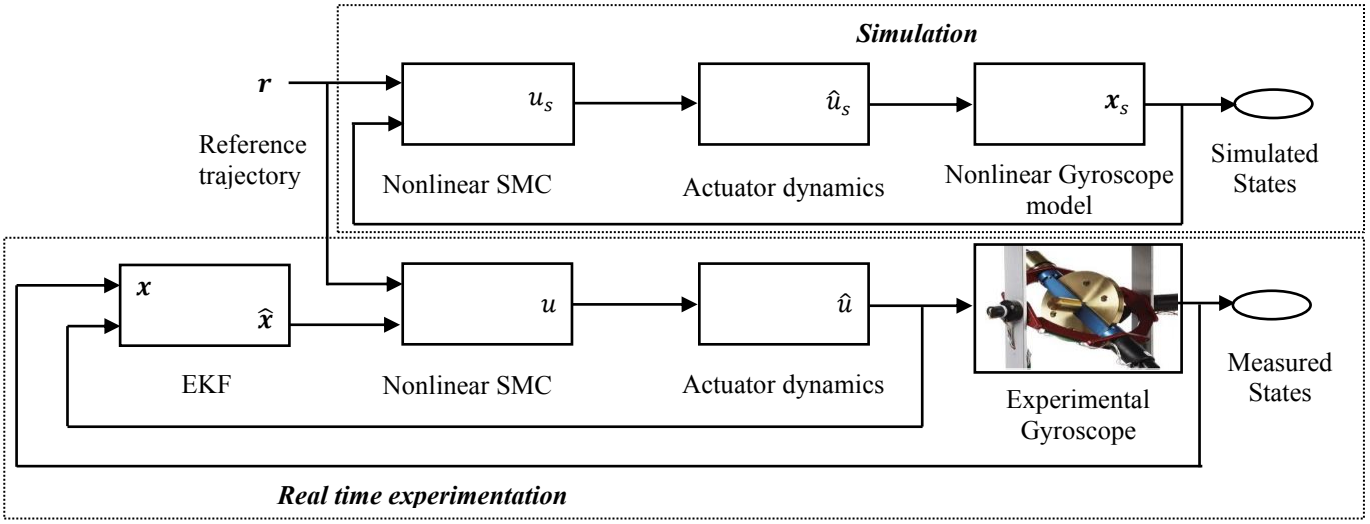

Fig. 2 Block diagram of the proposed control scheme in closed-loop

4. RESULTS AND DISCUSSIONS

Experimental and simulation results are presented in this section to evaluate the efficacy of the proposed closed-loop framework in the presence of uncertainties. Firstly, response of the experimental gyroscope setup to nonlinear SMC is considered. Then the performance of the proposed EKF based SMC framework on the gyroscope setup is evaluated.

4.1 Formulated SMC in closed-loop

Reference trajectory, ψ_d is retained at zero for $t = 20$ s to account for any discrepancies during the initial release of gimbals as flywheel motor and counter weights should be pointed upwards with ψ and θ maintained at zero during the start of the experiment. After $t = 20$ s, a sinusoidal signal of amplitude 20 degrees and frequency 0.05 Hz is used as a reference trajectory. In order to ensure the robustness of the proposed scheme, extra mass of 50 g is added to the red gimbal. This would affect its moment of inertia thereby influencing the performance of the system. Furthermore, the outer rectangular frame of the gyroscope setup is not tightly fastened allowing nominal oscillations about its rotating axis which could be perceived a vibratory disturbance in the laboratory setup.

The tracking performance of the system for the above mentioned scenarios using nonlinear SMC formulation in closed-loop is plotted in Fig. 3. Tuning parameters in Eqs. (13) and (20) used for numerical simulation and experimentation is chosen by trial and error and is listed in Eq. (29),

$$\epsilon = 15, \beta = 0.8, k_1 = 35, k_2 = 1 \qquad (29)$$

From Fig. 3, it could be deduced that there is a marginal delay in tracking, when implemented on a real time gyroscope setup. Figure 4 shows that though the control torque, u required to execute the proposed time varying reference trajectory is bounded, it is substantial with high frequency variations throughout the course of tracking. This is primarily attributed to the induced vibratory disturbances which could not be handled by nonlinear SMC formulation as indicated in Fig. 5.

4.2 Formulated SMC in closed-loop with EKF

From the inferences established on implementing nonlinear SMC on the real time gyroscope setup, it could be judged that the controller is sensitive to mismatched uncertainties induced by vibratory disturbances. Thus in this section, performance of the proposed EKF based SMC formulation to estimate and handle mismatched uncertainties is demonstrated.

Tuning of parameters while implementing nonlinear SMC on real time systems is challenging and time consuming. Besides, tuning parameters deduced using simulation platform based on gyroscope model might not work for uncertain real time system. But with the incorporation of EKF, tuning becomes simpler as the effect of uncertainties are attenuated to great extent. This is a noteworthy benefit mainly for implementing nonlinear SMC on a physical systems which lacks the comfort of trial and error based tuning. Thus using this formulation, range of tuning parameters could be gauged from simulation platform and could then be applied on experimental setup.

Tracking performance of the experimental gyroscope setup with EKF and nonlinear SMC in closed-loop is presented in Fig. 6. It could be seen that the reference trajectory is tracked efficiently by both simulation platform and experimental setup. It is also evident that the proposed scheme is robust to disturbances which are forced into experimental setup in the form of mass addition to the red gimbal and nominal oscillations of the outer rectangular frame. It could also be seen that the controller is agile to the change of reference trajectory which accelerates the convergence of error signal to zero.

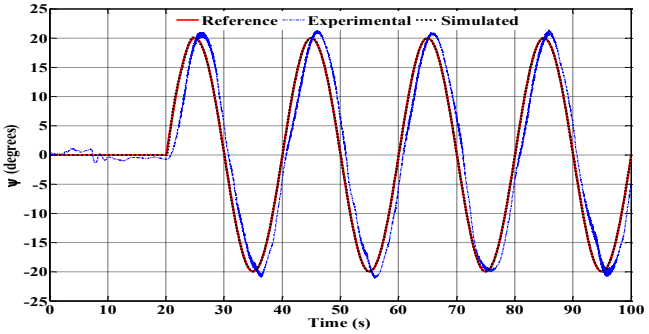

Fig. 3 Tracking performance with nonlinear SMC

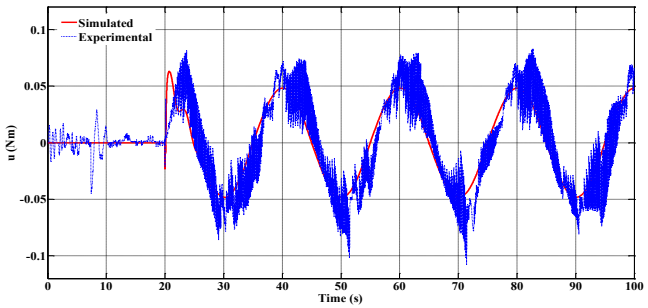

Fig. 4 Control input with nonlinear SMC

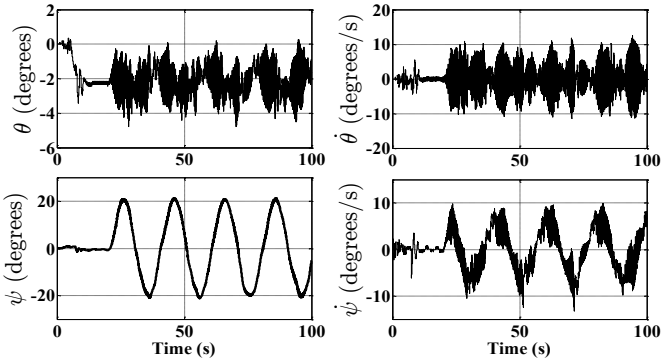

Fig. 5 State response with nonlinear SMC

Figure 7 represents the control torque, u required to achieve the tracking of the proposed reference trajectory. It is evident that the control signal is smooth and bounded. Besides, control torque generated in the case of real time gyroscope setup follows the trend of the control signal generated by the simulation platform. Though saturation limitation on actuator is imposed in the simulation platform, uncertain variables like rate limitation and delay are not enforced. This causes a small deviation of control torque generated by experimental setup in comparison with the simulated results, especially when rate of change of control signal is significant as inferred from Fig. 7.

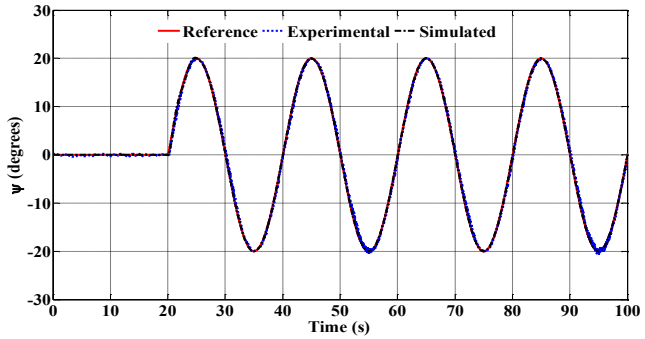

Fig. 6 Tracking performance with nonlinear SMC and EKF

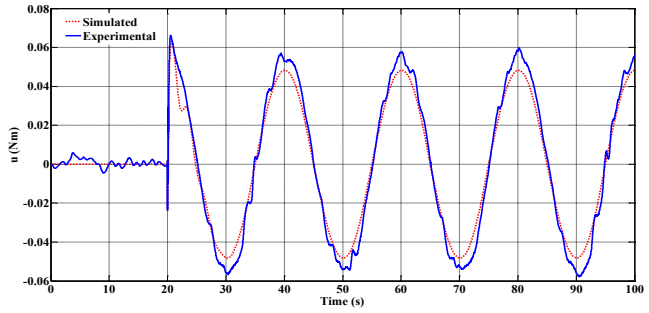

Fig. 7 Control input with nonlinear SMC and EKF

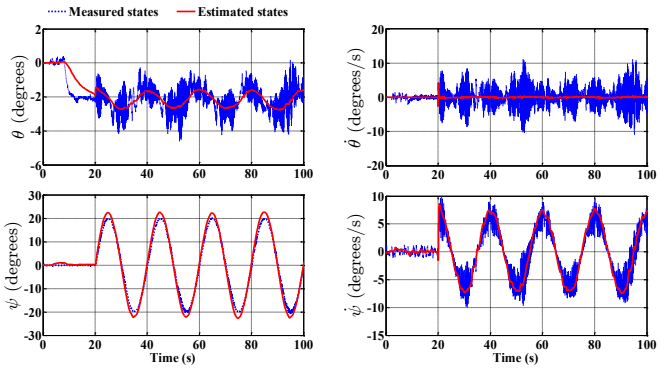

Fig. 8 State response with nonlinear SMC and EKF

Figure 8 depicts the response of states of gyroscope setup. Though all states are bounded, it is apparent that the measured states are highly influenced by induced uncertainties. Thus, EKF is employed to effectively handle both matched and mismatched uncertainties as inferred from Fig. 8. Thus, the proposed formulation with EKF and nonlinear SMC in closed-loop provides an enhanced asymptotically stable platform for robust, agile and precise control of real time gyroscope setup.

5. CONCLUSIONS

This work presents a methodical approach to the design and implementation of nonlinear control framework to real time systems with nonlinear SMC and EKF in closed-loop to handle both matched and mismatched uncertainties. Experimental evaluation successfully establishes the feasibility of implementation of proposed nonlinear formulation to real time systems affected by uncertainties. This facilitates upfront control of physical systems which are predominantly nonlinear, as piecewise linearization and control could be quite challenging and time consuming in most real world systems and might not capture some intriguing phenomena like chaos, limit cycles etc.

REFERENCES

Cannon Jr., R.H., (2003). *Dynamics of Physical Systems.* Dover Publications, New York.

Elkhayat, M.A., Elhalwagy, Y.Z., Elraffie, A.Y., Elnashar, G.A., (2016). Backstepping control using Single Gimbal Control Moment Gyro with parameter uncertainties. *In. IEEE Aerospace Conference,* Montana, 2016, 1–9.

Gao, W., Hung, J.C., (1993). Variable Structure Control of Nonlinear Systems: A New Approach. *IEEE Trans. Ind. Electron.* 40(1), 45–55.

Hou, L., Wang, L., Wang, H., (2017). SMC for Systems with Matched and Mismatched Uncertainties and Disturbances Based on NDOB. *Acta Autom. Sin.* 43(7), 1257–1264.

Jin, J., Hwang, I., (2012). Attitude Control of a Spacecraft with Single Variable-Speed Control Moment Gyroscope. *J. Guid. Control. Dyn.* 34(6), 1920–1925.

Khatri, A.K., Singh, J., Sinha, N.K., (2012). Aircraft Maneuver Design Using Bifurcation Analysis and Sliding Mode Control Techniques. *J. Guid. Control. Dyn.* 35(5), 1435–1449.

Lee, J.H., Ricker, N.L., (1994). Extended Kalman Filter Based Nonlinear Model Predictive Control. *Ind. Eng. Chem. Res.* 33(6), 1530–1541.

Leeghim, H., Kim, D., (2015). Adaptive neural control of spacecraft using control moment gyros. *Adv. Sp. Res.* 55(5), 1382–1393.

Montoya-Cháirez, J., Santibáñez, V., Moreno-Valenzuela, J., (2019). Adaptive control schemes applied to a control moment gyroscope of 2 degrees of freedom. *Mechatronics* 57, 73–85.

Naderolasli, A., Tabatabaei, M., (2017). Stabilization of the Two-Axis Gimbal System Based on an Adaptive Fractional-Order Sliding-Mode Controller. *IETE J. Res.* 63(1), 124–133.

Oliveira, T.R., Peixoto, A.J., Hsu, L., (2015). Global tracking for a class of uncertain nonlinear systems with unknown sign-switching control direction by output feedback. *Int. J. Control* 88(9), 1895–1910.

Sastry, S., (1999). *Nonlinear Systems: Analysis, Stability and Control.* Springer, New York.

Singh, S.N., (1989). Asymptotically Decoupled Discontinuous Control of Systems and Nonlinear Aircraft Maneuver. *IEEE Trans. Aerosp. Electron. Syst.* 25(3), 380–391.

Slotine, J.-J., Li, W., (1991). *Applied Nonlinear Control.* Prentice-Hall, New Jersey.

Stevenson, D., Schaub, H., (2012). Nonlinear control analysis of a Double-Gimbal Variable-speed control moment gyro. *J. Guid. Control. Dyn.* 35(3), 787–793.

Yang, J., Li, S., Yu, X., (2013). Sliding-mode control for systems with mismatched uncertainties via a disturbance observer. *IEEE Trans. Ind. Electron.* 60(1), 160–169.

Yu, C., Xie, X., (2019). Dynamic sliding mode-based attitude stabilisation control of satellites with angular velocity and control constraints. *Trans. Inst. Meas. Control* 41(4), 934–941.

Zhang, H., Fang, J., (2013). Robust Backstepping Control for Agile Satellite Using Double-Gimbal Variable-Speed Control Moment Gyroscope. *J. Guid. Control. Dyn.* 36(5), 1356–1363.